

View Article Online
View Journal

# Journal of Materials Chemistry A

Materials for energy and sustainability

# Accepted Manuscript

This article can be cited before page numbers have been issued, to do this please use: C. D. Redondo-Obispo, F. Serrano, J. Rubio-Zuazo, A. de Andres and C. Coya, *J. Mater. Chem. A*, 2025, DOI: 10.1039/D5TA05147A.



This is an Accepted Manuscript, which has been through the Royal Society of Chemistry peer review process and has been accepted for publication.

Accepted Manuscripts are published online shortly after acceptance, before technical editing, formatting and proof reading. Using this free service, authors can make their results available to the community, in citable form, before we publish the edited article. We will replace this Accepted Manuscript with the edited and formatted Advance Article as soon as it is available.

You can find more information about Accepted Manuscripts in the <u>Information for Authors</u>.

Please note that technical editing may introduce minor changes to the text and/or graphics, which may alter content. The journal's standard <u>Terms & Conditions</u> and the <u>Ethical guidelines</u> still apply. In no event shall the Royal Society of Chemistry be held responsible for any errors or omissions in this Accepted Manuscript or any consequences arising from the use of any information it contains.



Dpen Access Article. Published on 20 October 2025. Downloaded on 10/26/2025 8:38:17 PM.

This article is licensed under a Creative Commons Attribution-NonCommercial 3:0 Unported Licence

View Article Online DOI: 10.1039/D5TA05147A

## **ARTICLE**

Received 00th January 20xx, Accepted 00th January 20xx

DOI: 10.1039/x0xx000000x

# Radiation induced structural phase transition and damage in methyl ammonium lead perovskites studied by focused-beam synchrotron X-ray diffraction

Carlos D. Redondo-Obispo<sup>a</sup>, Federico Serrano-Sánchez<sup>a</sup>, Juan Rubio-Zuazo<sup>a,b</sup>, Alicia de Andrés<sup>a\*</sup> and Carmen Coya<sup>c\*</sup>

We investigate the structural degradation of methylammonium lead iodide (MAPbl<sub>3</sub>) thin films under focused hard X-ray (10 keV, 5×1013 ph/s/mm2) and violet laser (3.06 eV, 8×1017 ph/s/mm2) irradiation using synchrotron X-ray diffraction. The perovskites undergo a complex degradation landscape under irradiation charcterized by marked structural transformations, including phase decomposition into Pbl<sub>2</sub>, increased disorder, crystallite size reduction across all phases, loss of preferential orientation, and the unexpected formation of an orthorhombic MAPbI<sub>3</sub> phase. This new phase coexists with the original tetragonal structure, highlighting a novel irradiation-driven phase transition pathway. Photon flux (ph/s/mm²) rather than radiation flux (W/mm²) is the crucial parameter that triggers the partial phase transition to the orthorhombic structure which presents anomalously large lattice parameters. The transition is proposed to be activated by radiation-induced ion migration to lattice interstitial sites which restrict MA motion reducing entropy and locally increasing the orthorhombic transition temperature. This orthorhombic phase is surprisingly robust against radiation compared to the tetragonal one. Bi3+ doped MAPbl<sub>3</sub> presents higher disorder and smaller crystal size due to the heterovalent doping but, while radiation partially ablate the perovskite, Pbl2 formation is inhibited due to the preferred formation of Bil3. A CVD-deposited overlayer of Bil3 on MAPbl3 offers effective protection against combined X-ray and laser damage. These results advance our understanding of radiationinduced degradation in hybrid perovskites, revealing a previously unrecognized structural transformation pathway and highlighting that photon energy and fluence govern distinct and competing degradation mechanisms with potential implications for the stability and performance of perovskite-based optoelectronic devices.

#### 1. Introduction

Hybrid organic-inorganic perovskites (HOIPs), such as methylammonium lead iodide (MAPbI<sub>3</sub>), have rapidly positioned themselves at the forefront of materials research for next-generation optoelectronic devices, including solar cells,<sup>1</sup> light-emitting diodes,<sup>2</sup> photodetectors,<sup>3</sup> and lasers.<sup>4</sup> More recently, HOIPs have ventured into emerging fields such as neuromorphic computing, where they function as artificial synapses and memristors. <sup>5</sup> In addition, owing to the high atomic number of the constituting elements, strong absorption capabilities, and exceptional charge transport properties, high-energy radiation detection applications, including X-rays, γ-rays,

Electromagnetic irradiation from visible to X-rays can induce significant modifications in MAPbl<sub>3</sub> films, including ion migration, defect formation, and phase degradation.<sup>11</sup> This instability becomes even more critical under exposure to high-flux radiation, where the effects on the structural integrity and optoelectronic performance of MAPbl<sub>3</sub> remain insufficiently studied. Visible irradiation, especially short wavelengths, can lead to different effects on the structure of the material.<sup>12</sup> Previous work reported the degradation in air of MAPbl<sub>3</sub> into Pbl<sub>2</sub> in the presence of moisture (water) or PbO<sub>x</sub> under high flux laser visible irradiation in air.<sup>13</sup> The studies on the impact of X-ray radiation on perovskite films report a variety of results revealing the relevance of the characteristics of the beam (energy and flux) and the experiment conditions, such as exposure time and atmosphere (moisture and oxygen versus inert such as He, Ar or N).

and neutrons, have been demonstrated.6,7,8,9 Despite these remarkable advancements, the long-term structural and chemical stability of HOIPs under operational conditions remains a major challenge across all application, raising concerns about their reliability. Their vulnerability to degradation under solar irradiation is particularly critical for its use in photovoltaic and other light-driven applications.<sup>10</sup>

a. Instituto de Ciencia de Materiales de Madrid, Consejo Superior de Investigaciones Científicas, C/ Sor Juana Inés de la Cruz 3, 28049 Madrid Spain.

b. BM25-SpLine The Spanish CRG Beamline at the ESRF, Grenoble, 38043 Cedex 9, France

<sup>&</sup>lt;sup>c</sup> Escuela de Ingeniería de Fuenlabrada (EIF), Universidad Rey Juan Carlos, C/ Camino del Molino №5, 28942 - Fuenlabrada — Madrid, Spain.

<sup>\*</sup> Corresponding authors. A. de Andrés: <a href="mailto:ada@icmm.csic.es">ada@icmm.csic.es</a>, C. Coya: <a href="mailto:carmen.coya@urjc.es">carmen.coya@urjc.es</a>

Supplementary Information available: Figures of the Williamson-Hall plots, patterns for the analysis of PbI2 preferential orientation, different fits for the most degraded films and rocking curves. See DOI: 10.1039/x0xx00000x

ARTICLE Journal Name

The studies are mainly focused on the degradation evaluated by the reduction of the perovskite signal and eventual increase of Pbl<sub>2</sub> by different techniques such as XPS or XRD. Synchrotron X-ray sources, due to their high photon flux, and particularly when focused, are especially likely to induce damage in perovskite films<sup>1415</sup>. It is then necessary to investigate the response of HOIPs to synchrotron radiation that can provide valuable insights into their structural evolution, stability, and resilience, offering a deeper understanding of their potential for long-term operation in harsh environments. Although complete devices comprise multiple layers, the intrinsic stability of the active perovskite layer remains fundamental. Understanding these effects on MAPbl<sub>3</sub> is essential for both fundamental and applied research.

Several studies have employed synchrotron X-ray radiation (XRD) to study HOIPs, as Nam-Koo et al. 16 that used in-situ grazing-incidence wide-angle synchrotron XRD (GIWAXS) and high-resolution X-ray photoelectron spectroscopy (HR-XPS) to examine the thermal degradation of MAPbI<sub>3</sub> solar cells under controlled air-free conditions (no moisture or oxygen). Their results revealed the decomposition of the perovskite structure into CH3I, NH3, and PbI2 and changes in the orientation of CH<sub>3</sub>NH<sub>3</sub><sup>+</sup> cations. Renita et al.<sup>17</sup> used in situ GIWAXS to follow the structural changes that occur as the result of X-ray exposure (15.12 keV) of MAPbI<sub>3-x</sub>Br<sub>x</sub>. They observed that radiation-induced damage led to increased structural disorder, including the formation of ion vacancies and Schottky defects, almost independently from composition and relative humidity. X-ray irradiation studies at 7 keV under different atmospheres, including ambient air, inert gases, and vacuum, reported structural degradation in air, with minimal changes under dry N<sub>2</sub>.<sup>10</sup> In contrast, Holland et al., <sup>18</sup> observed structural degradation at 15.2 keV in both, ambient air and inert atmospheres, whereas a stabilization and self-healing of the perovskite lattice were noted in vacuum conditions.

The effects of radiation on HOIPs are complex and not yet fully established. Deeper investigation is essential for ensuring the reliability and long term performance of their many emerging applications. Herein we analyze the effect of micro-focused 10 keV X-rays on perovskites, as well as that of violet light (3.06 eV), that simulates an accelerated exposure to sunlight, using X-ray diffraction at the European Synchrotron Radiation Facility (ESRF). investigate the impact of radiation on MAPbI<sub>3</sub> films as well as in Bismuth (Bi) modified MAPbI<sub>3</sub> in two different ways: Bi-doped MAPbI<sub>3</sub>, where Bi<sup>3+</sup> is incorporated into the perovskite lattice, and MAPbl<sub>3</sub> films coated with a Bil<sub>3</sub> layer, proposed as a potential protective barrier against radiation-induced damage. Recent studies have explored various strategies to enhance the stability of MAPbI<sub>3</sub>, including chemical doping and surface passivation. 19 Bismuth doping has demonstrated remarkable effects showing an exceptional increase in photostability<sup>20,21</sup> and modifying its optical properties.<sup>22</sup> A comprehensive understanding of how synchrotron radiation differentially affects MAPbI<sub>3</sub>, Bi-doped MAPbI<sub>3</sub>, and BiI<sub>3</sub>-coated MAPbl₃ is presented.

#### 2. Experimental

#### 2.1 Materials

All materials are reagent grade and are used as received, Percyskite precursors are lead iodide (PbI<sub>2</sub>, 99.999% from Sigma-Aldrich), bismuth iodide (BiI<sub>3</sub>, 99.999% from Sigma-Aldrich) and methylammonium iodide (MAI or  $CH_3NH_3I$ , 98% from DYESOL). The solvent used are dimethyl formamide (DMF anhydrous 99.9%) and dimethyl sulfoxide (DMSO anhydrous 99.9%) from Sigma-Aldrich, and toluene ( $C_6H_5CH_3$ , 99.8%) from Alfa Aesar.

#### 2.2 Sample fabrication

Perovskite solutions preparation: A 25 wt% MAPbl $_3$  precursor solution was prepared by dissolving equimolar amounts of Pbl $_2$  and MAI in a 4:1 (v/v) DMF:DMSO mixture under stirring at 90 °C until complete dissolution. Bi-doped MAPbl $_3$  (MAPb $_{0.73}$ Bi $_{0.18}$ I $_3$ ) was synthesized following the procedure in Ref. 20. For this, Pbl $_2$ , Bil $_3$ , and MAI were mixed in anhydrous DMF to obtain a 25 wt% solution, stirred overnight at 60 °C, and then heated to 90 °C for 30 minutes prior to filtration. All solutions were filtered through 0.2  $\mu$ m hydrophilic PTFE syringe filters.

**Perovskite thin film preparation:** Precursor solutions and 2x2 cm size glass substrates were maintained at  $60 \, ^{\circ}\text{C}$  before the deposition process. The MAPbl<sub>3</sub> solution is deposited at 1000 rpm for 10 s, and 5000 rpm for 30 s. At 20 s of the second step, an antisolvent (toluene) is added in a volume three times of the perovskite.

 $MAPbI_3$ :Bi perovskite thin films are deposited at 1500 rpm for 45 s without antisolvent step and immediately transferred onto a hot plate at 100 °C for 60 min to finish perovskite crystallization.

MAPbl<sub>3</sub> layer/Bil<sub>3</sub> layer structure. Bil<sub>3</sub> layer is deposited by Chemical Vapor Deposition (CVT). A representative scheme is shown in Figure 1. A spin-coated MAPbl<sub>3</sub> thin film on a glass substrate was placed at one end of a 40 cm quartz tube furnace. At the opposite end, 10 mg of Bil<sub>3</sub> powder was positioned. Once the furnace reached 270 °C, the Bil<sub>3</sub> precursor is located into the central heating zone, allowing its sublimation and subsequent diffusion toward the film. The evaporation lasts 20 minutes under an Argon flux (P=5.8x10<sup>-1</sup> mbar) at a substrate temperature of 110 °C. This is the minimum temperature that allows the appropriate Bil<sub>3</sub> deposition.

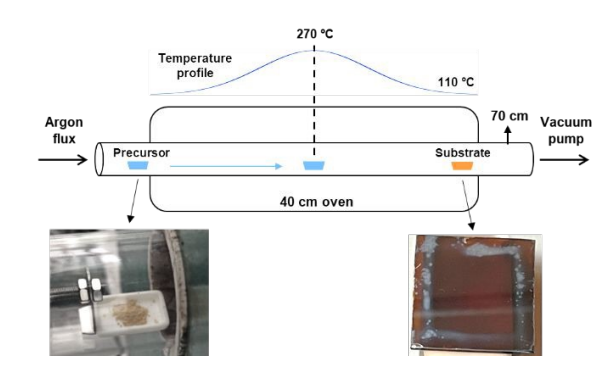


Figure 1. Scheme of Bil<sub>3</sub> deposition onto a spin-coated MAPbl<sub>3</sub> film.

#### 2.3 Film characterization

**Optical characterization:** For UV–vis absorption, a UV–Vis–NIR spectrophotometer (Varian, Cary 5000) in the wavelength range of 300–900 nm was used.

X-ray diffraction: Measurements were carried out at the SpLine CRG BM25 beamline at the European Synchrotron Radiation Facility (ESRF, Grenoble, France) in a six-circle diffractometer in vertical

Journal Name ARTICLE

geometry with a 2D hybrid pixel detector and a Si(111) monochromator, with an energy resolution of  $\Delta E/E \sim 10^{-4}$ . Measurements were performed at 10 keV with a focused beam of  $^{\sim}50 \times 50 \ \mu\text{m}^2$  (V  $\times$  H) at the sample position and a flux around 5 x 10<sup>13</sup> ph/s/mm<sup>2</sup>. The slits before the detector were either set to provide high angular resolution (narrowest measured peak width: 0.015°, estimated instrumental width: ~ 0.008°) or to provide high intensity at the expense of resolution. The relevant scans are detector scans with a fixed incident angle of 5°. For each film, the sample height is optimized to locate the sample at the center of the diffractometer, and it is localized with x and y-directions scans at the (110) perovskite diffraction peak. The diffraction data were analyzed using the Le Bail method in the model of the FullProf software.<sup>23</sup> The refined parameters as included are the following: scale factor, zeropoint error, background coefficients, pseudo-Voigt profile parameters, and lattice parameters.

#### 3. Results and Discussion

#### 3.1 MAPbl<sub>3</sub> films

This article is licensed under a Creative Commons Attribution-NonCommercial 3.0 Unported Licence

Open Access Article. Published on 20 October 2025. Downloaded on 10/26/2025 8:38:17 PM

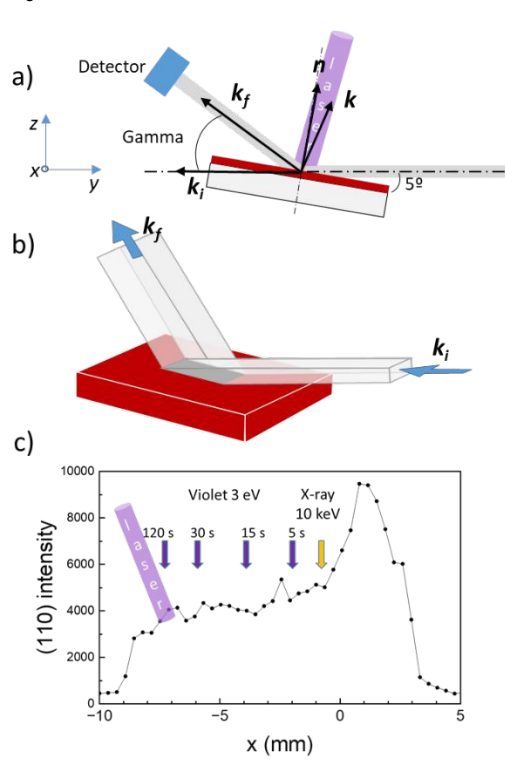


**Figure 2.** a) Measurement geometry: fixed incident angle at 5° and 10 keV.  $k_i$ ,  $k_f$  and k: incident, final and transferred momenta, n: surface normal vector; the laser beam is represented in violet; b) schema of the incident and diffracted beams and fingerprint (dark grey) of the beam; c) profile of the (110) MAPbl<sub>3</sub> peak intensity along the x axis, the positions where the patterns were measured are indicated.

The study of the structural modifications induced by hard X-ray (10 keV) and visible (3.06 eV) irradiation on MAPbI $_3$  films is presented here. The experimental configuration is schematized in **Figure 2**a and 2b. To ensure a constant irradiated area throughout the entire pattern collection, the incident angle was fixed to 5°. The focused X-

ray beam was reduced to 50  $\mu$ m  $\times$  50  $\mu$ m (horizontal (x)  $\times$  vertical (z) directions), enabling the analysis of the localized:impace of স-শ্রভ্যঞ্জর violet irradiations on the diffraction patterns. Consequently, the size of the observed area under the X-rays was around 50 μm x 580 μm on the sample. Additionally, a continuous N<sub>2</sub> flux directed onto the sample was used during the measurements so most of moisture and oxygen were displaced out from the sample. A profile of the (110) peak intensity was recorded across the sample along the x axis in 360 µm steps (Figure 2c) showing intensity variations of approximately 25% at the sub-mm scale, along with a significant increase on the right side related the thicker edge of ca. 3 mm wide. These variations reveal the thickness inhomogeneity of the spin-coated films due to the accumulation of the precursors at the edges of the substrate on one hand, and to different packing of the grains that leads to density variation along the film, on the other. The thickness of the films is in the range 320-350 nm. Similar profiles were obtained for all samples.

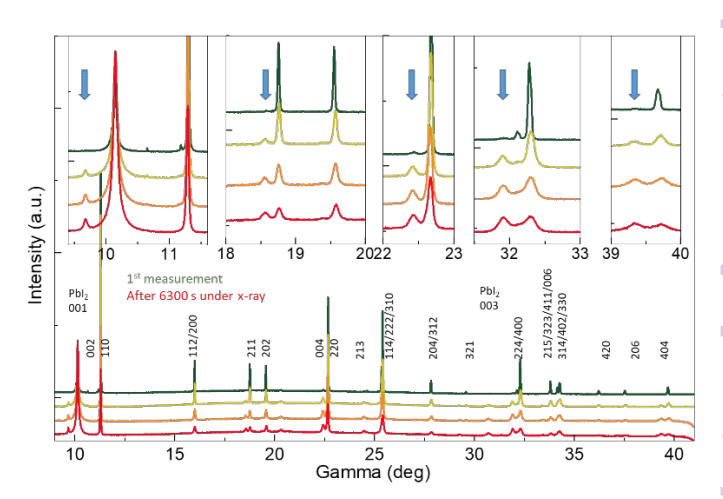


**Figure 3.** Diffraction patterns corresponding to successive measurements obtained at the same position within the MAPbl<sub>3</sub> film showing the effect of 10 keV irradiation time after 0, 900, 3800 and 6300 s (olive green, yellow, orange and red, respectively). Blue arrows indicate the extra peaks formed upon irradiation. The peaks are indexed to the I4/mcm tetragonal phase.

To evaluate the damage induced by the focused X-ray beam with a flux around 5 x 10<sup>13</sup> ph/s/mm<sup>2</sup>, successive measurements were done at the same sample position indicated in Figure 2c (yellow arrow). In this case the slits of the detector were reduced to reach the maximum angular resolution due to the extremely narrow peaks of the pristine films (< 0.015° for the (110) reflection). Figure 3 shows the diffraction patterns recorded after several irradiation times with insets highlighting relevant angular regions. The initial diffraction pattern was well fitted by including PbI<sub>2</sub> and tetragonal MAPbI<sub>3</sub> phases. Due to the highly textured nature of the films and the diffraction geometry, a profile-matching approach (Le Bail fit) was employed, as Rietveld refinement did not yield convergent results. The perovskite peaks of the pristine films are indexed to the I4/mcm (SG:140) tetragonal space group, and the (001)  $Pbl_2$  ( $P\overline{3}m1$ , SG:164) peak is labeled in Figure 3. Additional diffraction peaks appearing upon irradiation are indicated with blue arrows.

To analyze the preferential orientation of the grains of PbI<sub>2</sub> and MAPbI<sub>3</sub> phases it is important to consider that the fixed 5° incident angle almost satisfies the  $\theta$  -  $2\theta$  condition for the PbI<sub>2</sub> (001) peak and

ARTICLE Journal Name

closely approximates that of the MAPbI<sub>3</sub> (110) peak. Thus, for these peaks, the transferred vector (k) is almost parallel to the normal surface vector (n). It is then clear that the films present a preferential orientation of the grains along the planes (hh0) parallel to the substrate, as usual for these films1320 and the extremely low intensities of the (002) (at 11.1825°) and (004) (at 22.440°) diffraction peaks (Figure 3 a and c) indicate that the film is almost fully textured in the [110] direction. The rocking curve on the (110) peak is around 5º and allows the detection of other orientations whose intensities are larger as the angle  $\Phi$  between their wavevector and  $\mathbf{k}$  is smaller. According to Toraya empiric formula<sup>24</sup>, the probability of a reflection with angle  $\Phi$  is:  $p(\Phi) = P_1 + (1-P_1).exp(-P_2\Phi^2)$  where  $P_1$  is defined by the relative intensity of the perpendicular reflection, in this case (002), to the main orientation (110), while  $P_2$  is related to the width of the rocking curve of the (110) reflection. The domain size perpendicular to the film, obtained from the (110) MAPbl<sub>3</sub> peak, is > 320 nm for the pristine film (the width of this peak is limited by the instrumental function, see Figure S1 in S.I.) that coincides well with the perovskite film thickness of 345 nm.

Pbl<sub>2</sub> is fully textured in the [001] direction as no other diffraction peaks are detected which also indicates a very narrow direction distribution of the grains around [001]. This full texture can only be explained by the formation of PbI<sub>2</sub> grains localized at the substrate/perovskite interface. The domain size for PbI<sub>2</sub>, obtained from the (001) reflection, is 110 nm, which is surprisingly large considering the low intensity of the peak. Because of the different degrees of preferential orientation of the two phases it is not straightforward to evaluate their fractions within the film <sup>25</sup> and, unfortunately, Rietveld fitting could not be used. A rough estimate, obtained parametrizing the preferential orientation of both phases with the Toraya approximation, gives a PbI<sub>2</sub> content of around 2% in the film at this stage. These observations indicate that large Pbl<sub>2</sub> grains originate at discrete nucleation sites on the substrate during the synthesis of the MAPbI<sub>3</sub> films. The fraction of substrate covered by Pbl<sub>2</sub>, calculated considering the film thickness (345 nm) and 110 nm tall PbI<sub>2</sub> grains, is therefore around 10%. This originates the observed fluctuations of the PbI<sub>2</sub> intensity in the micro-focus XRD patterns at the beam area scale (tens of µm). A schematic representation of the pristine sample evolution under X-ray irradiation is shown in Figure 4, from the first measurement (left panel) to the irradiated state (right panel).

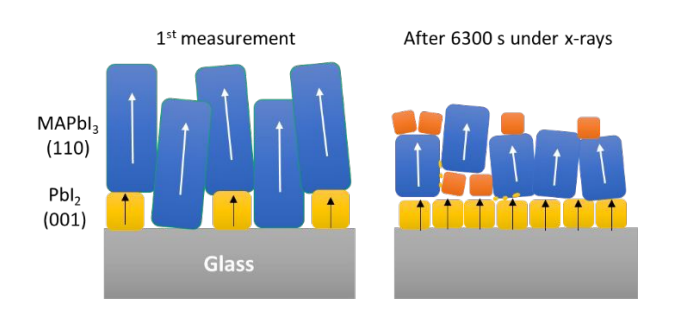


**Figure 4** Sketch of the MAPbI<sub>3</sub> film before and after 6300" under X-ray irradiation according to XRD results. White arrows correspond to (110) preferential orientation of the tetragonal perovskite and black arrows to that of PbI<sub>2</sub> along (001). The relative sizes of the drawn grains correspond to the XRD domain sizes. The orange grains represent the orthorhombic MAPbI<sub>3</sub> phase.

Hard X-ray irradiation induces several notable changes in the diffraction patterns: a general broadening of all peaks, an increase in

the intensity of the Pbl<sub>2</sub> phase, a reduction in the perceyskite peaks intensity, and the appearance of additional: reflections AOFhese effects—particularly the broadening of perovskite peaks and the contrasting evolution of the two main phases—are clearly evidenced in the insets of Figure 3. The concurrent decrease in MAPbl<sub>3</sub> peak intensity and increase in Pbl<sub>2</sub> signal provide clear evidence of perovskite degradation, likely involving the loss of volatile methylammonium species. In addition, the emergence of new diffraction peaks (indicated by arrows in Figure 3) suggests the formation of a secondary phase induced by X-ray exposure.

Regarding the PbI<sub>2</sub> phase, it maintains its (001) orientation after irradiation. In Figure S2 (see the S.I.), calculated patterns for polycrystalline and fully textured (001) PbI<sub>2</sub> are shown together with the measured patterns highlighting the PbI<sub>2</sub> peaks. At the position of the (011) Pbl<sub>2</sub> refection (at 20.62°), which is the most intense in powder samples, an extremely weak feature is discerned after irradiation (see inset of Figure S2 c). In order to maintain the almost full preferential orientation, the (001) Pbl<sub>2</sub> grains promoted by X-rays must be localized at the substrate/perovskite interface. The extremely weak peaks corresponding to reflections ≠ (001) (Figure S2 c and insets) could be associated to the existence of PbI<sub>2</sub> nanoparticles at the perovskite-film grain boundaries, however the similar width of these peaks to those of the (001) reflections has to be interpreted as being originated by grains with a small deviation from the strict (001) direction rather than to PbI<sub>2</sub> nanoparticles since these would produce significantly wider peaks. The existence of a small fraction of tiny and/or highly disordered Pbl2 regions, however, cannot be discarded even if no clear signal is detected by XRD.

The broadening of diffraction peaks upon X-ray irradiation observed for both MHP and PbI<sub>2</sub> phases can be originated by microstrain, distortion, disorder and defects as well as by the reduction of the domain size. In the case of PbI<sub>2</sub>, the grain size reduction was estimated using the width of the sole intense peak. This is a good approximation since the impact of strain on the width of low-k peaks is small. For the tetragonal MAPbI<sub>3</sub> phase, the Williamson-Hall (W-H) plot method is used to analyze the observed broadening<sup>26</sup> (plots in Figure S1 in SI). The W-H plots were obtained using the widths of the profile matching fits and indicate a broadening caused by crystal size reduction (vertical shift) and by a significant increase of defects and stress in the structure (slope).<sup>27</sup> The MAPbI<sub>3</sub> film in its initial stage exhibits feeble microstrain that is more than doubled after 6300 s under X-rays. The obtained microstrain values are overestimated since the sample is being modified while measuring. i.e. the width of the peaks is increased as the scan proceeds due to the disorder induced by the X-ray probe itself. This is important and should be considered, as sample modification during the measurement limits the feasibility of long focused-beam synchrotron XRD studies on this type of compounds.

Thus, to minimize the impact of X-rays on the evaluation of visible light irradiation using XRD, it is necessary to irradiate the film at different positions in the sample for several time intervals. The reference pattern is the same as the previously presented in the X-ray irradiation time-dependent study. The patterns of the MAPbl<sub>3</sub> film before and after several violet (3.06 eV) laser irradiation times, from 5s to 120 s, at the locations indicated in Figure 2c were obtained and those for 30s and 120s are shown in Figure 5. In this case, the key effect is the formation of the same new peaks detected after long X-ray irradiation, evidenced after only 5 s of violet irradiation.

This article is licensed under a Creative Commons Attribution-NonCommercial 3.0 Unported Licence

Open Access Article. Published on 20 October 2025. Downloaded on 10/26/2025 8:38:17 PM

**Journal Name ARTICLE** 

However, in this case, the PbI<sub>2</sub> phase fraction e shows little variation and the broadening of the perovskite peaks is minor after 120 s of violet irradiation. The diffraction intensities of MAPbl<sub>3</sub> and Pbl<sub>2</sub> peaks present some fluctuations along the samples, caused by the previously mentioned morphological inhomogeneities. These variations hinder a precise comparison of intensities arising from different points, but the observed trends are reliable.

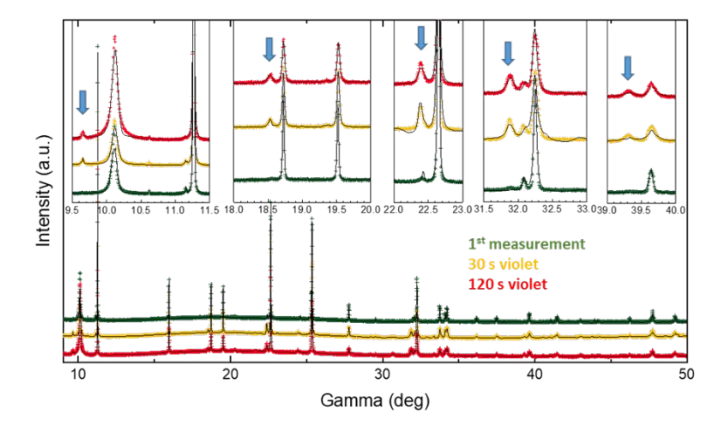


Figure 5 Patterns at different positions: pristine (olive), after 30s (orange) and 120 s (red) of violet, 3.06 eV, illumination. The black lines correspond to profile fits to tetragonal I4/mcm MAPbI3 and PbI2 phases. An orthorhombic Pnma MAPbI<sub>3</sub> phase is included in the fit, defining the new appearing peaks after irradiation (blue arrows).

To account for the additional diffraction peaks, several possibilities were considered, including standard phases such as hydrated MAPbI<sub>3</sub>, double perovskites, lead oxides, and precursor compounds. Structural models involving symmetry reduction to the orthorhombic space group Pnma or the coexistence of two tetragonal MAPbl<sub>3</sub> phases with different lattice parameters and preferred orientations were also tested. Representative fits for several of these scenarios are shown in Figure S3. While the peaks at 18.55, 22.4 and 31.9° correspond well to the alpha phase of PbO<sub>2</sub> <sup>28</sup>, in particular to the (110), (111) and (221) reflections, other emerging peaks of similar characteristics (width and evolution with radiation) do not match with this phase. The rapid diffusion of O2 within the MAPbI3 films has been reported and is explained to be accompanied by the photo-induced formation of highly reactive O2-29 that initiate the perovskite degradation forming PbI<sub>2</sub> and I<sub>2</sub>.<sup>30</sup> Moreover, PbO<sub>2</sub> phase has been identified by Raman spectroscopy as a degradation product of 2.54 eV laser irradiation in low relative humidity atmosphere (50%) while the formation of PbI<sub>2</sub> requires higher humidity or longer times.13 In this case the use of N2 flux on the sample during the measurements seems to inhibit the formation of lead oxide. The profile fits of the diffraction patterns (Figure 4) show that violet radiation readily induces the transformation of a fraction of the perovskite grains to an orthorhombic structure with the same space group, Pnma, as the low temperature phase observed bellow 160 K in this compound<sup>31</sup>, showing significantly larger lattice parameters,  $a_0$  = 8.951(5),  $b_0$ = 8.986(7) and  $c_0$ = 12.666(6) Å (Figure 6). The unit cell volume is 8.6 % larger than for the tetragonal phase.

Unfortunately, the profile fits do not allow the determination of the atomic positions of the ions within the cell. DOI: 10.1039/D5TA05147A

The in-phase octahedral rotational angle  $\boldsymbol{\theta}$ , is evaluated using the approximation:  $heta = \cos^{-1}(b/\sqrt{2ac})^{32}$  to compare the here identified Pnma phase with the standard one induced at low temperature. The obtained values,  $\theta = 3.29^{\circ}$  and 3.48° for samples irradiated 2 min at 3.06 eV and 105 min at 10 keV, respectively, are significantly smaller compared to that of the low-temperature Pnma structure at ≈8.7°.31 It should be noted that the formula assumes rigid, undistorted octahedra thus systematically underestimating the rotation. Importantly, the a and b lattice parameters in our RT Pnma structure are much closer in length than those at low temperature (a = 8.8115, b = 8.5597 Å at 10 K,<sup>31</sup> consistent with a lower distortion in the irradiated Pnma phase compared to the intrinsic lowtemperature phase.

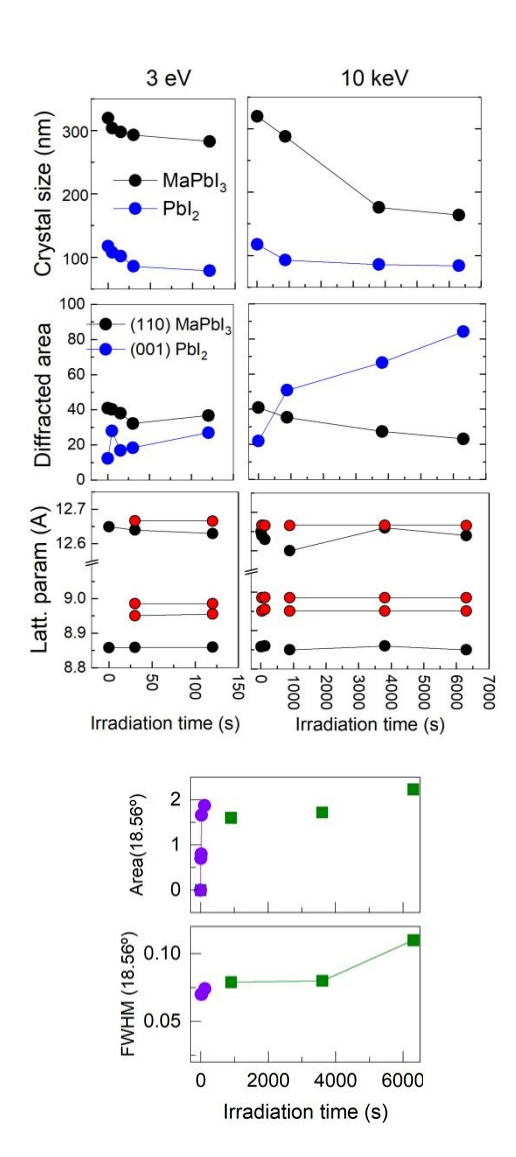


Figure 6. Upper panels: evolution with 3.06 eV and 10 keV irradiation time of tetragonal MAPbI<sub>3</sub> (black circles), PbI<sub>2</sub> (blue circles) and orthorhombic MAPbI<sub>3</sub> (red circles) phases: crystal size, (110) and (001) diffraction peak intensities and lattice parameters. Lower

**Journal Name** 

This article is licensed under a Creative Commons Attribution-NonCommercial 3.0 Unported Licence

Open Access Article. Published on 20 October 2025. Downloaded on 10/26/2025 8:38:17 PM

panels: area and width of the 18.56° peak of the orthorhombic phase under 3.06 eV (violet dots) and 10 keV (green squares) radiation.

The top panels of Figure 6 show the variation of domain size and areas of the (001) Pbl<sub>2</sub> reflection and that corresponding to the (110) peak of tetragonal MAPbl<sub>3</sub> after different 10 keV and 3.06 eV irradiation times. It evidences that X-ray exposition produces important damage on MAPbl<sub>3</sub> at long times. The short time evolution under 3.06 eV violet radiation shows the dynamics of the initial degradation stage. Violet laser irradiation, with an estimated power density of 40 W/cm² here, simulates an accelerated solar induced degradation. Pbl<sub>2</sub> peak at 10.3° reveals a rapid and quite important domain size reduction at 30 s that reaches 36% in 2 minutes, while for MAPbl<sub>3</sub> it is reduced only 10%. The intensities of both phases vary slightly for these violet irradiation times. However, the rapid surge of the spurious phase, monitored by the intensity of the 18.56° new peak, is clear in the lower panels of Figure 5 where violet dots correspond to violet irradiation and green squares to X-rays.

The dynamics and characteristics of the orthorhombic phase are interesting: the phase is formed after only 5 s of 3.06 eV irradiation and the peak width shows the dominating presence of large grains (90 nm). The intensity of the orthorhombic peaks remains almost constant for longer violet irradiation times and the PbI<sub>2</sub> phase fraction also remains constant. The transformation into the orthorhombic phase is slower when irradiated with X-rays and, while no further significant increased intensity is detected, its domain size is progressively reduced. Therefore, the irradiation first effect consists in the fast light-induced transformation of a fraction of the tetragonal MAPbI<sub>3</sub> grains into large orthorhombic ones. Visible light at 3.06 eV presents a strong optical absorption that induces this modification of the perovskite structure much more efficiently than X-rays, which primarily cause random disorder. The formation of Pbl<sub>2</sub> is accelerated by X-rays being a much slower process than the partial phase transition. The violet laser has four orders of magnitude more photon flux than the X-ray beam but the energy of the photons are almost four orders of magnitude less. The power densities of both sources are therefore similar (40 W/cm<sup>2</sup> for the laser and 90 W/cm<sup>2</sup> for the x-ray beam). This indicates that the energy of the violet photons is enough to promote the phase transition, and the photon flux (ph/s/mm<sup>2</sup>) is the relevant parameter while the high energy of the much less numerous x-ray photons mainly produce disorder at short times.

The changes in lattice parameters of the tetragonal phase are small with an initial decrease of  $c_T$  and a subsequent increase after 880 s as damage proceeds (the lattice parameters vary from  $a_O$  = 8.858(5) and  $c_O$ = 12.65(2) to  $a_O$  = 8.850(13) and  $c_O$ = 12.64(6) for the most damaged sample). This is probably related to the induced disorder. including the displacement of ions at interstitials, either as iodide or as neutral iodine ( $I_I^X$ ) which is smaller in size and easily photogenerated<sup>33</sup>, while  $a_T$  remains almost constant. Figure 6 illustrates the changes occurring in the films according to the obtained results: the domain sizes of PbI<sub>2</sub> and the MHP phases are reduced, PbI<sub>2</sub> extends at the perovskite/substrate interface and large perovskite domains are transformed into PbI<sub>2</sub> and orthorhombic MAPbI<sub>3</sub>.

Irradiation, either with X-rays or light also yield a reduction of the preferential orientation of the tetragonal phase, ኯዕብ 100% የሪክ ተክê non-irradiated pattern to 60% / 15% for the 120 s violet / 6300 s Xray irradiated cases, respectively. Considering the recently proposed mechanism for the tetragonal to orthorhombic phase transition<sup>34</sup>, the observed loss of crystallographic orientation appears to correspond to the initial stages of this transition. The phase transition was described as a sequence of Pb-I octahedra tilting that induces small rotation of adjoining MA+, occurring with an overall very low effective energy barrier. In this process, the rotational entropy of MA<sup>+</sup> cations regulates the transition temperature. We propose that radiation promotes the rotation Pb-I octahedra, which in turn acts as a trigger for the phase transition. The subtle equilibrium between the two phases may also be modified by radiation induced point defects. The notable unit cell volume increase from the tetragonal ( $\sim$  992 Å<sup>3</sup>) to the orthorhombic ( $\sim$  1079 Å<sup>3</sup>) structures, may reveal the presence of interstitial ions that block the MA+ cation rotation lowering their contribution to entropy and therefore modifying the equilibrium between the two phases. An inhomogeneous distribution of the generated interstitials would favor locally the phase transition to the orthorhombic structure. The here proposed mechanism for the room temperature tetragonal to orthorhombic phase transition is well supported by the theoretical study by Li W. et al35 whose calculations indicate that iodine interstitials not only create a large distortion in the Pb-I octahedra, they also constrain the rotation of the adjacent MA molecules. The stability of the diffraction peaks intensity of this orthorhombic structure (see evolution of the 18.563 peak area in Figure 6) is extraordinary compared to the regular tetragonal one (see (110) evolution in the same figure).

Finally, the changes in the tetragonal MAPbl $_3$  and Pbl $_2$  phase fractions are also likely due to radiation reinforced diffusion of I and Pb ions. The migration of both species is required to promote the growth of the Pbl $_2$  layer at the MAPbl $_3$ / substrate interface.

#### 3.2 MAPbl<sub>3</sub>:Bi and MAPbl<sub>3</sub>/Bil<sub>3</sub>

One of our objectives was obtaining the local structural changes occurring upon focused-high density laser irradiation, done previously in our laboratory under previously established conditions<sup>20</sup>, on Bi<sup>3+</sup>-doped MAPbl<sub>3</sub> films. The typical extension of the laser-modified region is 300 microns that we showed to present distinct properties compared to the non-irradiated films.<sup>20</sup> However, despite the focused synchrotron X-ray beam, the large extension of the X-ray trace in the *y* direction and especially the degradation occurring during the XRD measurements did not allow the detection and analysis of these modified micro-regions. Alternatively, we evaluate the effect of i) Bi<sup>3+</sup> doping and ii) Bil<sub>3</sub> coating of MAPbl<sub>3</sub>, on the degradation of the perovskite upon X-ray irradiation (Figure 7).

Journal Name ARTICLE

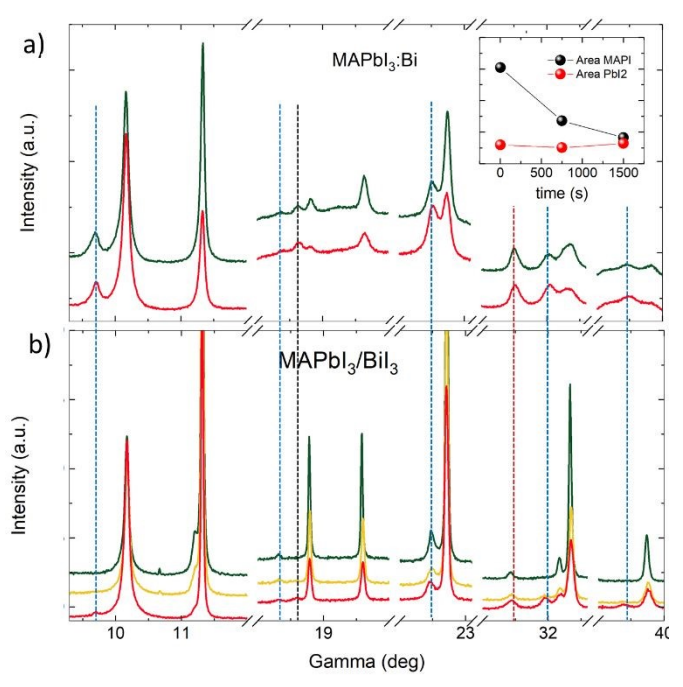
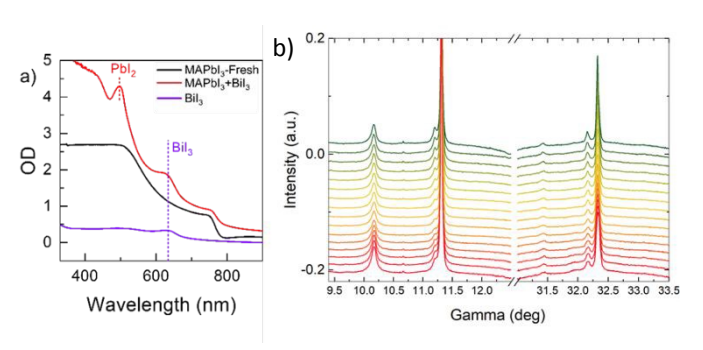


Figure 7 Diffraction patterns of a) MAPbl<sub>3</sub>:Bi film before (green) and after (red) 1440 s x-ray, 10 keV, irradiation at the same position of the film. Blue dashed lines indicate the peaks related the orthorhombic phase and black to Bil<sub>3</sub> phase. The inset shows the evolution of the areas of perovskite (110) and (001) Pbl<sub>2</sub> peaks. b) Initial pattern for MAPbl<sub>3</sub>/Bil<sub>3</sub> film (green) and after two successive measurements while being continuously irradiated with the violet laser.

Bi doping produces an important widening of the diffraction peaks due to the distortion associated with charge compensation, since trivalent Bi substitutes divalent Pb ions, and a reduction of the domain size (around 90 nm). The films also present a lower preferential orientation than undoped ones. These characteristics lead to much weaker diffraction patterns. Figure 7a shows the relevant regions of the XRD patterns for a Bi doped MAPI<sub>3</sub> film before and after 1440 s of 10 keV irradiation. The extra peaks assigned to the orthorhombic phase of MAPbI<sub>3</sub> are found in the pristine film (dashed blue lines) with little variation upon irradiation but with different relative intensities compared to the undoped case, the peaks at 9.7° and 22.5° are stronger. Additionally, an intense peak at 31.5° and a weak one at 19.4° are detected. The 22.5° peak may also correspond to Bil<sub>3</sub> precursor (explaining its intensity) as well as that at 31.5°. The intensity of the Bil<sub>3</sub> peaks vary along the film at the submillimeter scale indicating some inhomogeneity in the Bil<sub>3</sub> phase.

Bi doped MAPI<sub>3</sub> films show some particularities upon irradiation compared to undoped films. In particular, Bi doping seems to inhibit the formation of PbI<sub>2</sub> under X-ray irradiation. The inset of Figure 6 shows that PbI<sub>2</sub> phase is almost constant while the perovskite does degrade significantly. This is most probably related to the presence of Bi that traps lodine forming BiI<sub>3</sub>. This BiI<sub>3</sub> phase shows a small increase upon perovskite degradation. The widths of the rocking curves of different peaks indicate a very narrow orientation

distribution of the grains for (110) (FWHM  $\sim$  4°) and (220) (FWHM  $\sim$  5°) while a polycrystalline character is found for the (200) Field (Figure S4). The films are therefore a combination of textured grains and a polycrystalline fraction. The effect of X-ray radiation is opposite for the (004) and (224) reflections than for the (220) and (400) peaks. For the first peaks, intensity increases while it is reduced for the later. The (220) and (400) peaks correspond to the oriented grains and the (004) and (224) (closer to the (001) direction) are mainly related the polycrystalline fraction. It seems then that the oriented grains are more sensitive to X-rays contrary to the polycrystalline fraction that increases as a result of this damage.



**Figure 8** a) Absorbance of a MAPbI<sub>3</sub> film before (black line) and after (red line) evaporation of a BiI<sub>3</sub> over-layer and of a BiI<sub>3</sub> film on glass (violet line); b) evolution of two relevant angular regions of the diffraction patterns of a BiI<sub>3</sub>/MAPbI<sub>3</sub> film under X-rays at 90" intervals (total: 1440"=24")

The effect of an ultra-thin Bil<sub>3</sub> layer on a MAPbl<sub>3</sub> film is then evaluated. A Bil<sub>3</sub> layer was deposited by CVT on spin-coated MAPbl<sub>3</sub> films as described in the experimental section. The formation of a Bil<sub>3</sub> layer is confirmed in the absorption spectra. Figure 8a shows the spectra of a pristine MAPbl<sub>3</sub> film, a MAPbl<sub>3</sub> film with a thick Bil<sub>3</sub> layer deposited by CVT on top and a reference Bil<sub>3</sub> film. The thickness of the Bil<sub>3</sub> used for the diffraction experiments was reduced so that the characteristic feature around 630 nm of Bil<sub>3</sub> is almost indistinguishable. The high deposition temperature, 110 °C, favors the formation of Pbl<sub>2</sub>, which is especially important for the sample with a thick Bil<sub>3</sub> layer shown in Figure 8a, but the perovskite crystalline structure is preserved.

The deposited Bil<sub>3</sub> layer protects the MAPbl<sub>3</sub> film from degradation as can be observed in Figure 8b (pristine and up to 24' under X-ray irradiation). Little variations in peak widths and areas are observed in this time scale. The sample was then measured under simultaneous and continuous violet laser irradiation to enhance the damage (Figure 7b). After 30 minutes the Pbl<sub>2</sub> phase shows some increment and the MAPBl<sub>3</sub> peak area some decrease. Hints of the orthorhombic phase are then detected and Bil<sub>3</sub> peaks at 22.5° and 31.4°, which are already seen in the pristine film, slightly increase upon irradiation. The observed degradation is significantly reduced with the Bil<sub>3</sub> over-layer, even combining X-ray and laser irradiation.

#### **Conclusions**

ARTICLE Journal Name

Synchrotron microfocus X-ray diffraction experiments reveal inhomogeneity in thickness and density along MAPbI<sub>3</sub> films deposited on glass by spin coating. Texture analysis reveals an almost complete (110) preferential orientation of the tetragonal grains with crystal size perpendicular to the substrate matching the film thickness. The small fraction of PbI<sub>2</sub> phase initially present in the films is fully (100) textured, features large crystal size (around 90 nm) and an estimated substrate coverage < 10 %. The measurement itself damages the films after a few minutes for 10 keV beam with a photon flux  $\sim 5 \times 10^{13}$  ph/s/mm<sup>2</sup>. X-ray irradiation at short times (minutes) mainly produces disorder, reduces the crystal size of all compounds and phases and favors the degradation of the tetragonal perovskite structure, accelerating ionic diffusion resulting in the formation of fully (100) oriented PbI<sub>2</sub> grains. We propose that the radiation induced PbI<sub>2</sub> grains are confined at the substrate/perovskite interface.

Violet (3.06 eV) laser irradiation, with a much higher photon flux (8×10<sup>17</sup> ph/s/mm<sup>2</sup>) but a lower radiation flux than the focused X-ray beam (40 W/cm<sup>2</sup> compared to 90 W/cm<sup>2</sup> for X-rays), after only 5 s, locally induces a phase transition of the MAPbI<sub>3</sub> perovskite from the I4/mcm tetragonal structure to an orthorhombic phase with the same space group (Pnma) as the one below 160 K in a fraction of the film. The X-ray beam also induces this phase transformation at longer times. This orthorhombic structure presents anomalously large lattice parameters that may originate from the presence of a certain density of interstitial ions promoted by radiation. We propose that these interstitials could hinder, by steric constraints, the well-known MA rotations occurring at room temperature thus reducing the entropy energy. The appropriate entropy reduction, occurring in some crystals within the film, triggers their structural transition to the orthorhombic phase at room temperature. The out of plane crystal size of this phase is large > 90 nm and only long x-ray irradiation time is able to reduce it. Additional X-ray irradiation induces disorder also in this phase but does not reduce its intensity within the measured time range, up to 105 min, while the tetragonal phase continuously decreases, evidencing the robustness of the orthorhombic

Doping this perovskite with  $Bi^{3+}$  significantly inhibits the formation of  $Pbl_2$  and the transition to the orthorhombic phase during irradiation and but still the tetragonal phase is ablated. The formation of  $Bil_3$  appears to be more favourable compared than that of  $Pbl_2$ . Finally coating  $MaPbl_3$  films with a CVD-deposited  $Bil_3$  extremely thin layer provides an effective radiation shielding even with the simultaneous use of X-ray and violet laser.

#### **Author contributions**

Conceptualization: AdA, C.C; Formal Analysis: all; Investigation: all; Resources: CC; supervision: AdA, CC; writing-original draft: AdA, CC; writing-review&editing: all.

#### Conflicts of interest

View Article Online DOI: 10.1039/D5TA05147A

There are no conflicts to declare.

### Data availability

The data that support the findings of this study are included in the article and in the Supporting Information file.

#### Acknowledgements

This work was funded by Rey Juan Carlos University (URJC) under project F1259. We also acknowledge the MINECO for Financial support and provision of synchrotron radiation facilities at ESRF and thank beamline BM25-SpLine for technical support. C.R.-O. acknowledges Spanish Ministry of Science and Innovation for FPI pre-doctoral contract grant (PRE2019-088433).

#### Notes and references

- M. Jeong, I. W. Choi, E. M. Go, Y. Cho, M. Kim, B. Lee, S. Jeong, Y. Jo, H. W. Choi, J. Lee, J.-H. Bae, S. K. Kwak, D. S. Kim and C. Yang, *Science* (1979), 2020, 369, 1615–1620.
- Z. Liu, W. Qiu, X. Peng, G. Sun, X. Liu, D. Liu, Z. Li, F. He, C.
   Shen, Q. Gu, F. Ma, H. Yip, L. Hou, Z. Qi and S. Su, *Advanced Materials*, 2021, 33, 2103268.
- 3 L. Dou, Y. Yang, J. You, Z. Hong, W.-H. Chang, G. Li and Y. Yang, *Nat Commun*, 2014, **5**, 5404.
- 4 G. Lee, B. P. Rand and K. Roh, ACS Appl Mater Interfaces,
- J. Choi, J. Su Han, K. Hong, S. Young Kim, H. Won Jang, J. Choi, J. S. Han, K. Hong, H. W. Jang and S. Y. Kim, *Advanced Materials*, 2018, 30, 1704002.
- 6 L. Zhang, L. Mei, K. Wang, Y. Lv, S. Zhang, Y. Lian, X. Liu, Z. Ma, G. Xiao, Q. Liu, S. Zhai, S. Zhang, G. Liu, L. Yuan, B. Guo, Z. Chen, K. Wei, A. Liu, S. Yue, G. Niu, X. Pan, J. Sun, Y. Hua, W.-Q. Wu, D. Di, B. Zhao, J. Tian, Z. Wang, Y. Yang, L. Chu, M. Yuan, H. Zeng, H.-L. Yip, K. Yan, W. Xu, L. Zhu, W. Zhang, G. Xing, F. Gao and L. Ding, Nanomicro Lett, 2023, 15, 177.
- Y. He, I. Hadar and M. G. Kanatzidis, *Nature Photonics 2021* 16:1, 2021, 16, 14–26.
- S. Deumel, A. van Breemen, G. Gelinck, B. Peeters, J. Maas, R. Verbeek, S. Shanmugam, H. Akkerman, E. Meulenkamp, J. E. Huerdler, M. Acharya, M. García-Batlle, O. Almora, A. Guerrero, G. Garcia-Belmonte, W. Heiss, O. Schmidt and S. F. Tedde, *Nature Electronics 2021 4:9*, 2021, **4**, 681–688.

**Journal Name** 

This article is licensed under a Creative Commons Attribution-NonCommercial 3.0 Unported Licence

pen Access Article. Published on 20 October 2025. Downloaded on 10/26/2025 8:38:17 PM

9 H. Wei and J. Huang, *Nature Communications 2019 10:1*,

- 9 H. Wei and J. Huang, *Nature Communications 2019 10:1*, 2019, **10**, 1–12.
- F. M. C. da Silva, R. Szostak, V. C. Teixeira, J. C. Germino, M.
   M. Soares, A. F. Nogueira and H. C. N. Tolentino, *Solar RRL*, 2023, 7, 2200898.
- M. E. Stuckelberger, T. Nietzold, B. M. West, Y. Luo, X. Li, J. Werner, B. Niesen, C. Ballif, V. Rose, D. P. Fenning and M. I. Bertoni, *Journal of Physical Chemistry C*, 2020, **124**, 17949–17956.
- M. Ouafi, B. Jaber, L. Atourki, R. Bekkari and L. Laânab, J Alloys Compd, 2018, 746, 391–398.
- E. Climent-Pascual, B. C. Hames, J. S. Moreno-Ramírez, A. L. Álvarez, E. J. Juarez-Perez, E. Mas-Marza, I. Mora-Seró, A. De Andrés and C. Coya, *J Mater Chem A Mater*, 2016, 4, 18153–18163.
- 14 R. L. Z. Hoye, P. Schulz, L. T. Schelhas, A. M. Holder, K. H. Stone, J. D. Perkins, D. Vigil-Fowler, S. Siol, D. O. Scanlon, A. Zakutayev, A. Walsh, I. C. Smith, B. C. Melot, R. C. Kurchin, Y. Wang, J. Shi, F. C. Marques, J. J. Berry, W. Tumas, S. Lany, V. Stevanović, M. F. Toney and T. Buonassisi, *Chemistry of Materials*, 2017, **29**, 1964–1988.
- F. M. C. da Silva, R. Szostak, M. G. D. Guaita, V. C. Teixeira,
   A. F. Nogueira and H. C. N. Tolentino, *Energy Materials*,
   2024, 4, 400058.
- 16 N. K. Kim, Y. H. Min, S. Noh, E. Cho, G. Jeong, M. Joo, S. W. Ahn, J. S. Lee, S. Kim, K. Ihm, H. Ahn, Y. Kang, H. S. Lee and D. Kim, *Scientific Reports* 2017 7:1, 2017, 7, 1–9.
- 17 R. M. D'Souza and T. L. Kelly, *ACS Mater Lett*, 2023, **5**, 3222–3228.
- 18 M. Holland, A. Ruth, K. Mielczarek, V. V. Dhas, J. J. Berry and M. D. Irwin, ACS Appl Mater Interfaces, 2022, 14, 9352–9362.
- S. Sandhu and N.-G. Park, Acc Mater Res, 2024, 5, 1544–
   1557.
- J. Bartolomé, E. Climent-Pascual, C. Redondo-Obispo, C. Zaldo, Á. L. Álvarez, A. De Andrés and C. Coya, *Chemistry of Materials*, 2019, 31, 3662–3671.
- J. Marí-Guaita, A. Bouich and B. Marí, *JOM*, 2022, **74**, 3103–3110.
- C. Redondo-Obispo, I. Suárez, S. J. Quesada, T. S. Ripolles, J.
   P. Martínez-Pastor, A. L. Álvarez, A. de Andrés and C. Coya,
   J Phys Chem Lett, 2020, 11, 2188–2194.

J. Rodríguez-Carvajal, *Physica B Condens Matter*, 1993, 2001; 10.1039/D5TA05147A
 DOI: 10.1039/D5TA05147A

**ARTICLE** 

- 24 H. TORAYA and F. MARUMO, *Mineralogical Journal*, 1981, 10, 211–221.
- 25 C. Redondo-Obispo, P. Serafini, E. Climent-Pascual, T. S. Ripolles, I. Mora-Seró, A. De Andrés and C. Coya, ACS Appl Energy Mater, 2021, 4, 13943–13951.
- S. A. Hassanzadeh-Tabrizi, J Alloys Compd, 2023, 968, 171914.
- 27 T. Ungár, Scr Mater, 2004, **51**, 777–781.
- S. Filatov, N. Bendeliani, B. Albert, J. Kopf, T. Dyuzeva and
   L. Lityagina, *Solid State Sci*, 2005, 7, 1363–1368.
- N. Aristidou, C. Eames, I. Sanchez-Molina, X. Bu, J. Kosco,
   M. S. Islam and S. A. Haque, *Nat Commun*, 2017, 8, 15218.
- 30 N. Aristidou, I. Sanchez-Molina, T. Chotchuangchutchaval, M. Brown, L. Martinez, T. Rath and S. A. Haque, Angewandte Chemie International Edition, 2015, 54, 8208– 8212.
- P. S. Whitfield, N. Herron, W. E. Guise, K. Page, Y. Q. Cheng, I. Milas and M. K. Crawford, *Scientific Reports 2016 6:1*, 2016, **6**, 1–16.
- C. J. Howard and H. T. Stokes, Acta Crystallogr B, 1998, 54, 782–789.
- 33 G. Y. Kim, A. Senocrate, T. Y. Yang, G. Gregori, M. Grätzel and J. Maier, *Nature Materials 2018 17:5*, 2018, **17**, 445– 449.
- 34 J. Wu, J. Chen and H. Wang, JACS Au, 2023, 3, 1205–1212.
- 35 W. Li, J. Liu, F.-Q. Bai, H.-X. Zhang and O. V. Prezhdo, *ACS Energy Lett*, 2017, **2**, 1270–1278.

Data availability statement for the manuscript:

View Article Online DOI: 10.1039/D5TA05147A

"Radiation induced structural phase transition and damage in methyl ammonium lead perovskites studied by focused-beam synchrotron X-ray diffraction"

Authors: Carlos D. Redondo-Obispo, Federico Serrano-Sánchez, Juan Rubio-Zuazo, Alicia de Andrés and Carmen Coya

The data that support the findings of this study are included in the article and in the Supporting Information file.

The raw data will be uploaded in the "DIGITAL-CSIC· repository and a DOI will be provided.

Alicia de Andrés and Carmen Coya

Corresponding authors